



RESEARCH ARTICLE

Alpha-synuclein-associated changes in PINK1-PRKN-mediated mitophagy are disease context dependent

Xu Hou¹  | Taylor Hsuan-Yu Chen¹ | Shunsuke Koga¹  | Jenny M. Bredenberg¹ | Ayman H. Faroqi^{1,2} | Marion Delenclos¹ | Guojun Bu^{1,2} | Zbigniew K. Wszolek³ | Jonathan A. Carr⁴ | Owen A. Ross^{1,2} | Pamela J. McLean^{1,2} | Melissa E. Murray^{1,2} | Dennis W. Dickson^{1,2} | Fabienne C. Fiesel^{1,2} | Wolfdieter Springer^{1,2}

¹Department of Neuroscience, Mayo Clinic, Jacksonville, Florida, USA

²Neuroscience PhD Program, Mayo Clinic Graduate School of Biomedical Sciences, Jacksonville, Florida, USA

³Department of Neurology, Mayo Clinic, Jacksonville, Florida, USA

⁴Division of Neurology, Department of Medicine, Faculty of Medicine and Health Sciences, Stellenbosch University, Cape Town, South Africa

Correspondence

Wolfdieter Springer, Department of Neuroscience, Mayo Clinic, 4500 San Pablo Road, Jacksonville, FL 32224, USA.
Email: springer.wolfdieter@mayo.edu

Funding information

Alzheimer's Association, Grant/Award Number: AARF-22-973152; Congressionally Directed Medical Research Programs, Grant/Award Numbers: W81XWH-17-1-0248, W81XWH-17-1-0249; National Institute of Neurological Disorders and Stroke, Grant/Award Numbers: P30 AG062677, P50 NS072187, R01 NS078086, R01 NS085070, R01 NS110085, R56 AG062556, U19 AG063911, U54 NS100693, U54 NS110435

Abstract

Alpha-synuclein (α syn) aggregates are pathological features of several neurodegenerative conditions including Parkinson disease (PD), dementia with Lewy bodies, and multiple system atrophy (MSA). Accumulating evidence suggests that mitochondrial dysfunction and impairments of the autophagy-lysosomal system can contribute to the deposition of α syn, which in turn may interfere with health and function of these organelles in a potentially vicious cycle. Here we investigated a potential convergence of α syn with the PINK1-PRKN-mediated mitochondrial autophagy pathway in cell models, α syn transgenic mice, and human autopsy brain. PINK1 and PRKN identify and selectively label damaged mitochondria with phosphorylated ubiquitin (pS65-Ub) to mark them for degradation (mitophagy). We found that disease-causing multiplications of α syn resulted in accumulation of the ubiquitin ligase PRKN in cells. This effect could be normalized by starvation-induced autophagy activation and by CRISPR/Cas9-mediated α syn knockout. Upon acute mitochondrial damage, the increased levels of PRKN protein contributed to an enhanced pS65-Ub response. We further confirmed increased pS65-Ub-immunopositive signals in mouse brain with α syn overexpression and in post-mortem human disease brain. Of note, increased pS65-Ub was associated with neuronal Lewy body-type α syn pathology, but not glial cytoplasmic inclusions of α syn as seen in MSA. While our results add another layer of complexity to the crosstalk between α syn and the PINK1-PRKN pathway, distinct mechanisms may underlie in cells and brain tissue despite similar outcomes. Notwithstanding, our finding suggests that pS65-Ub may be useful as a biomarker to discriminate different synucleinopathies and may serve as a potential therapeutic target for Lewy body disease.

KEYWORDS

alpha-synuclein, autophagy, Lewy body disease, mitochondria, mitophagy, multiple system atrophy, Parkinson disease, phosphorylated ubiquitin, PINK1, PRKN

This is an open access article under the terms of the [Creative Commons Attribution](https://creativecommons.org/licenses/by/4.0/) License, which permits use, distribution and reproduction in any medium, provided the original work is properly cited.

© 2023 The Authors. *Brain Pathology* published by John Wiley & Sons Ltd on behalf of International Society of Neuropathology.

1 | INTRODUCTION

Parkinson disease (PD) is an incurable neurodegenerative disorder which is characterized by slow progression of the cardinal motor symptoms and the occurrence of comorbid, nonmotor symptoms as the disease develops [1]. Aside from significant loss of dopaminergic neurons and projections, the main pathological hallmark of PD is the abnormal accumulation of alpha-synuclein (α syn) in the form of Lewy bodies (LBs) and Lewy neurites within the surviving neurons [2]. α syn inclusions are also features of other neurodegenerative disorders, including, but not limited to, dementia with Lewy bodies and multiple system atrophy (MSA). While these diseases are collectively referred to as synucleinopathies, the affected brain regions and cell types as well as the distribution and morphology of α syn aggregates vary considerably [3].

Mitochondrial dysfunction is believed to be a major contributor to PD and has also been linked to MSA as the resulting energy deficits, oxidative stress, and impaired signaling are all known to promote the aggregation of α syn [4, 5]. Moreover, accumulation of α syn is likely also a consequence of impaired autophagic-lysosomal degradation [6, 7]. The main pathway for selective elimination of damaged mitochondria by autophagy (mitophagy) is orchestrated by the ubiquitin (Ub) kinase PINK1 and the Ub ligase PRKN [8]. Complete loss of either gene function causes early-onset PD and it is thought that the concomitant buildup of damaged mitochondria eventually leads to cell death. PINK1 continuously surveils mitochondrial health and accumulates only on depolarized mitochondrial membranes where it phosphorylates serine-65 of Ub (pS65-Ub). Binding to pS65-Ub recruits and activates the Ub ligase PRKN which provides additional substrates for PINK1 and thus amplifies the mitophagy signal [8]. Damaged mitochondria decorated with pS65-Ub are then subjected to the autophagic-lysosomal system for degradation.

A functional relationship between α syn aggregation and mitophagy alterations is emerging, but greater insights into this likely complex crosstalk and the underlying mechanisms have remained elusive [9]. It has been shown that loss of either PINK1 or PRKN can aggravate α syn-induced phenotypes [10–13], while overexpression of each enzyme can ameliorate those [14–18]. Furthermore, α syn was shown to impact mitochondria, autophagy, and lysosomes and thus could alter the mitophagy process at different steps, but perhaps also in different directions [7, 9, 19–24]. Cells and transgenic mice expressing A53T mutant α syn showed marked accumulation of mitochondria-containing autophagic vesicles [25, 26]. Certain α syn species were shown to strongly bind to the mitochondrial import receptor TOMM20, which could lead to mitophagy defects [27]. Another conformationally distinct, nonfibrillar form of α syn induced structural and functional mitochondrial damage leading to increased fission and enhanced mitophagy [28]. Altogether, this suggests that alterations of mitophagy may well play a key role in the α syn-related pathogenesis.

Since both lysosomal storage disorders and mitochondrial diseases appear disproportionately vulnerable to the deposition of LBs, the process of LB formation may be the consequence of dysfunctions in either of these organelles [29]. Indeed, LBs were recently shown to contain membranous components and organellar remnants, including mitochondria and lysosomes [30]. Previously we have already demonstrated the accumulation of the mitophagy marker pS65-Ub in Lewy body disease (LBD) cases, where the punctate structures colocalized with α syn signals and closely decorated the surface of LBs [31]. We here set out to further explore the complex interrelation between α syn and mitophagy, the potential underlying molecular mechanisms, and the pathological implications in different cell models, α syn transgenic mice, and in autopsy brain from cases with LBD or MSA.

2 | MATERIALS AND METHODS

2.1 | Collection, culture, and genetic or pharmacological manipulation of patient fibroblasts

Primary human dermal fibroblasts were collected from two *SNCA* triplication (*SNCA*x3) carriers, one *SNCA* duplication (*SNCA*x2) carrier, and their respective healthy siblings that served as controls. The collection, processing, and analyses of primary dermal fibroblast were approved by the Institutional Review Board at Mayo Clinic. All fibroblasts were cultured in Dulbecco's modified Eagle medium (Thermo Fisher, 11965118) supplemented with 10% fetal bovine serum (Neuromics, FBS001800112), 1% PenStrep (Thermo Fisher, 15140122), and 1% nonessential amino acids (Thermo Fisher, 11140050). Fibroblasts were grown at 37°C, 5% CO₂:air in humidified atmosphere. α syn knockout fibroblasts were generated by transducing cells with Lenti-CRISPRv2 vector (Addgene, Plasmid #52961) containing a single guide RNA targeting the *SNCA* start codon (TCCTTTCATGAATACATCCA) and followed by antibiotic selection. PRKN knockdown fibroblasts were generated by transfecting cells with siRNA (Qiagen, SI02661267) using nucleofection (Lonza, V4XP-2024). 20 μ g/mL cycloheximide (CHX, Sigma–Aldrich, C1988), 200 nM bafilomycin A1 (Cayman Chemicals, 11038), 1 μ M epoxomicin (Sigma, E3652), HBSS (Thermo Fisher, 14025076), 0.5 μ M valinomycin (Enzo Life Science, BML-KC140-0025), or vehicle DMSO (Sigma–Aldrich, D4540) were used for cell treatments.

2.2 | Direct conversion of fibroblasts to induced neurons

The *trans*-differentiation of fibroblasts into induced neurons (iNeurons) was performed as previously described with modifications [32, 33]. Briefly, primary patient

fibroblasts were seeded in 6-well plates and transduced with lentiviral particles containing human PTB shRNA for 48 h in the presence of 5 $\mu\text{g}/\text{mL}$ Polybrene (Sigma–Aldrich, TR-1003-G) at 32°C. Transduced cells were selected with 2 $\mu\text{g}/\text{mL}$ puromycin (Thermo Fisher, A1138-03) starting 2 days after transduction. Two days later, 10 ng/mL basic fibroblast growth factor (GenScript, Z02734) was added to the fibroblast media and cultivation continued for additional 2 days. From day 7 on, cells were maintained in differentiation medium containing DMEM/F12 (Thermo Fisher, 11320–082), 5% fetal bovine serum (NeuroMics, FBS001800112; further reduced to 2% after 2 days), 1% PenStrep (Thermo Fisher, 15140122), 25 $\mu\text{g}/\text{mL}$ insulin (Sigma–Aldrich, I9278), 100 nM putrescine (Sigma–Aldrich, P5780), 50 $\mu\text{g}/\text{mL}$ transferrin (Sigma–Aldrich, T8158), 30 nM sodium selenite (Sigma–Aldrich, S5261), and 15 ng/mL basic fibroblast growth factor. After 6 days, 2% B27 supplement without antioxidants (Thermo Fisher, 10889-038) and 10 ng/mL each of brain-derived neurotrophic factor (R&D Systems, 248-BD-025), glial cell-derived neurotrophic factor (R&D Systems, 212-GD-050), neurotensin-3 (Peprotech, AF-450-03), and ciliary neurotrophic factor (Peprotech, 450-13) were added to the differentiation medium. The cells were used for experiments 2 days later. Neuronal differentiation was confirmed by expression of the neuronal marker tubulin beta 3 class III (TUBB3).

2.3 | Maintenance and expression regulation of H4 cells

Stable human H4 neuroglioma cells expressing αsyn fusion proteins under a tetracycline-controlled transcriptional activation system [34] were provided by Dr. McLean (Mayo Clinic, Jacksonville, USA). H4 cells were grown in Opti-MEM reduced serum growth medium (Thermo Fisher, 51985091) supplemented with 10% fetal bovine serum, 200 $\mu\text{g}/\text{mL}$ of G418 (Thermo Fisher, 10131-035), 200 $\mu\text{g}/\text{mL}$ of hygromycin (Thermo Fisher, 10687010), and 1 $\mu\text{g}/\text{mL}$ of tetracycline (Sigma–Aldrich, T7660) at 37°C, 5% CO_2 :air in humidified atmosphere. To induce αsyn expression in H4 cells, tetracycline was removed from the culture medium.

2.4 | RNA extraction and real-time quantitative PCR

RNA was extracted from fibroblast cell pellets using a RNeasy Mini Kit (Qiagen, 74106). Real-time quantitative PCR was performed using iTaq Universal SYBR Green One-Step Kit (Bio-Rad, #1725150). Specifically, 50 ng of RNA was mixed with primers for the targeted genes (Table S1), SYBR Green, and iScript reverse transcriptase in a 5 μL reaction. The PCR was executed using a 384-well block on a LightCycler 480 system (Roche,

Switzerland). Relative transcript levels for targeted genes were calculated with $2^{-\Delta\Delta\text{CT}}$ method using RPL27 as housekeeping gene and normalized to the relative expression level of the control [35].

2.5 | Western blot

Cells were lysed in RIPA buffer (50 mM Tris, pH 8.0, 150 mM NaCl, 0.1% SDS, 0.5% deoxycholate, 1% NP-40) containing protease inhibitor cocktail and phosphatase inhibitors (Sigma–Aldrich, 11697498001 and 04906837001). Cell lysates were cleared for 15 min, 4°C at $20,817 \times g$ and protein concentrations were determined by BCA assay (Thermo Fisher, 23225). Cell lysates containing 15 μg of protein were diluted in Laemmli buffer (62.5 mM Tris, pH 6.8, 1.5% SDS, 8.33% glycerol, 1.5% β -Mercaptoethanol, 0.005% bromophenol blue) and boiled at 95°C for 5 min before running on Tris-Glycine gels (Invitrogen, EC60485BOX). Post transfer of protein onto PVDF membranes (Millipore Sigma, IPVH00010), membranes were blocked in 5% skim milk (Genesee, 20-241) and incubated with primary antibodies against αsyn (BD Biosciences, 610787; 1:2000), PRKN (Millipore, MAB5512; 1:5000), PINK1 (Cell Signaling Technology, 6946; 1:1000), TUBB3 (Cell Signaling Technology, 5568; 1:5000), LC3 (Novus Biologicals, NB100-2220; 1:10,000), GFP (Takara Bio, 632381; 1:10,000), cyclin dependent kinase inhibitor 1A (CDKN1A/P21) (Cell Signaling Technology, 2947; 1:2000), pS65-Ub (in-house, 1:10,000) [33], mitofusin 2 (MFN2) (Abcam, ab56889; 1:2000), GAPDH (Meridian Life Sciences, H86504M; 1:500,000), and vinculin (VCL) (Sigma–Aldrich, V9131; 1:500,000) overnight at 4°C, followed by secondary HRP-conjugated antibodies (Jackson ImmunoResearch, 711-035-152, 715-035-150, 115-035-207, 115-035-205; 1:10,000) for 1 h at room temperature. For αsyn immunoblotting, PVDF membranes were incubated with 4% paraformaldehyde (Sigma–Aldrich, 441244) containing 0.01% glutaraldehyde (Electron Microscopy Science, 16020) for 30 min at room temperature prior to blocking [36, 37]. Protein bands were visualized using Immobilon Western Chemiluminescent HRP Substrate (Millipore Sigma, WBKLS0500) and Blue Devil Lite X-ray films (Genesee Scientific, 30-810L).

2.6 | Immunofluorescence staining of iNeurons

To examine the neuronal structure, iNeurons were also differentiated on glass coverslips that were coated with growth-factor reduced matrigel (Millipore, CLS356252, 1:1000 in PBS). Cells were fixed with 4% paraformaldehyde, permeabilized with 1% Triton X-100, blocked with 10% goat serum, and incubated with primary antibody

against TUBB3 (Millipore, AB9354; 1:250) followed by incubation with secondary antibody (Invitrogen, A-11034; 1:1000) and Hoechst 33342 (Invitrogen, H21492; 1:5000). Coverslips were mounted onto microscope slides using fluorescent mounting medium (Dako, S302380-2). High-resolution confocal fluorescent images were taken with an AxioObserver microscope equipped with an ApoTome Imaging System (Zeiss, Oberkochen, Germany).

2.7 | Immunofluorescence staining of fibroblasts and high content imaging

To quantify pS65-Ub levels using automated high-content imaging, fibroblasts were seeded in 96-well imaging plates (Fisher Scientific, 08772225) and allowed to attach overnight. Cells were then treated for 0, 4, 8, or 24 h with 1 μ M valinomycin and fixed in 4% paraformaldehyde after one wash with PBS. Fibroblasts were immunostained with primary antibodies against pS65-Ub (Cell Signaling Technology, 62802; 1:1250) and HSP60 (arigo Biolaboratories, ARG10757; 1:2000) followed by incubation with secondary antibody (Invitrogen, A-11034 and A-11041; 1:1000) and Hoechst 33342 (Invitrogen, H21492; 1:5000). Plates were imaged on a BD Pathway 855 (BD Biosciences, San Jose, CA, USA) with a 20 \times objective using a 2 \times 2 montage (no gaps) with laser autofocus every second frame as previously described [33]. Raw images were processed using the built-in AttoVision V1.6 software. Regions of interest were defined as nucleus and cytoplasm using the built-in “RING-2 outputs” segmentation for the Hoechst channel after applying a shading algorithm. Values were normalized to 0 h and 24 h valinomycin treated control cells as 0% and 100%, respectively.

2.8 | Animal cohort and tissue collection

All procedures involving animals were in accordance with the ethical standards and approved by the Institutional Animal Care and Use Committee at Mayo Clinic. Brain tissue from 9 to 18 months old Line D mice ($n = 18$) that overexpress wild-type human α syn from the platelet-derived growth factor- β promoter [38] and their nontransgenic littermate controls ($n = 11$) were used. Mice were euthanized and transcardially perfused with PBS and then brains were quickly removed and fixed in 4% paraformaldehyde overnight. Fixed brain was then embedded in paraffin wax for sectioning.

2.9 | Human autopsy brain

All brain samples are from autopsies performed after approval by the legal next-of-kin. Research on de-

identified postmortem brain tissue is considered exempt from human subjects' regulations by the Mayo Clinic Institutional Review Board. In the current study, autopsy brains of neurologically normal controls ($n = 15$), LBD cases without known familial risk factors ($n = 9$), LBD cases with *SNCA* multiplications or missense mutations (LBD^{mut}, $n = 6$), and MSA-parkinsonian type (MSA-P) cases ($n = 15$) from non-Hispanic Caucasians were retrieved for immunohistochemical analyses from the Mayo Clinic Florida Brain Bank. All brains were examined in a systematic and standardized manner by a single neuropathologist, as previously described [39]. Available neuropathological information included age at death, sex, Braak neurofibrillary tangle stage (0–VI), and Thal amyloid phase (0–5) (see Table S2 and S3).

2.10 | Immunohistochemistry

Paraffin embedded brain tissue was cut into 5 μ m sections and allowed to dry overnight at 60°C. Slides were deparaffinized and rehydrated, followed by antigen retrieval in steaming deionized water for 30 min. After blocking with 0.03% hydrogen peroxide and 5% normal goat serum (Invitrogen, 16210072), sections were incubated with primary antibodies against pS65-Ub (in-house, 1:650) [31], α syn (for human brain: NACP [40], Mayo Clinic Jacksonville, 1:3000; for mouse brain: Thermo Scientific, MA1-90346, 4B12, 1:5000), or phospho-tau (CP13, gift from the late Dr. Peter Davies, Feinstein Institute, North Shore Hospital, NY, 1:1000), followed by rabbit- or mouse-labeled polymer HRP (Agilent, K4011 and K4007) at room temperature. For NACP staining, slides were pretreated with 98% formic acid for 30 min before steaming to retrieve the antigen. Peroxidase labeling was visualized with the chromogen solution 3,3'-diaminobenzidine (Agilent, K4011 and K4007). The sections were then counterstained with Lerner 1 hematoxylin (Fisher Scientific, CS400-1D) and coverslipped with Cytoseal mounting medium (Thermo Scientific, 8310). After immunohistochemical staining, all sections were scanned with an Aperio AT2 digital pathology scanner (Leica Biosystems, Wetzlar, Germany) and then traced and quantified using optimized Aperio algorithms to measure the total signal or count the positive cell number followed by manual quality control [31].

2.11 | Immunofluorescence and imaging human brain tissue

Following target retrieval and blocking, brain sections were incubated in primary antibodies against pS65-Ub (in-house, 1:650) and pS129- α syn (Wako Chemicals USA, 015-25191; 1:3000) at 4°C overnight and in secondary antibodies (Invitrogen, A-11034 and A-11004;

1:1000) with DAPI (Sigma–Aldrich, D9542; 1:1000) at room temperature for 1.5 h. 3% Sudan black (SPI Supplies, 02560-AB) was used to quench autofluorescence before slides were coverslipped in fluorescence mounting medium (Agilent, S302380). After immunofluorescence staining, super-resolution confocal (Airyscan) images were taken with a LSM 880 microscope (Zeiss, Oberkochen, Germany) with z-stack.

2.12 | Statistical analysis

Statistical analysis of cell experiments was performed with one-way ANOVA. For measures in animals, unpaired *t* tests were used. For human cohorts, given that most measures were not normally distributed and had differing variances between groups, nonparametric tests

(Kruskal–Wallis and Mann–Whitney *U* tests followed by adjustment with Bonferroni correction) were used. Statistical analyses were performed using GraphPad Prism (GraphPad Software; version 9).

3 | RESULTS

3.1 | Elevated α syn expression leads to an increase in PRKN protein across different cell types

To examine potential α syn-associated alterations in PINK1-PRKN-mediated mitophagy, we first assessed their gene expression in primary fibroblasts from three siblings, two of which carry a triplication of the *SNCA* locus. As expected, mRNA levels of *SNCA* were significantly increased in both triplication cell lines, albeit to different extent (Figure 1A). Neither *PINK1* nor *PRKN* transcription was changed in any of the cells. While it is known that fibroblasts generally have very low expression of *SNCA* [41, 42], both triplication cells showed more than 5–10 fold increased α syn protein levels

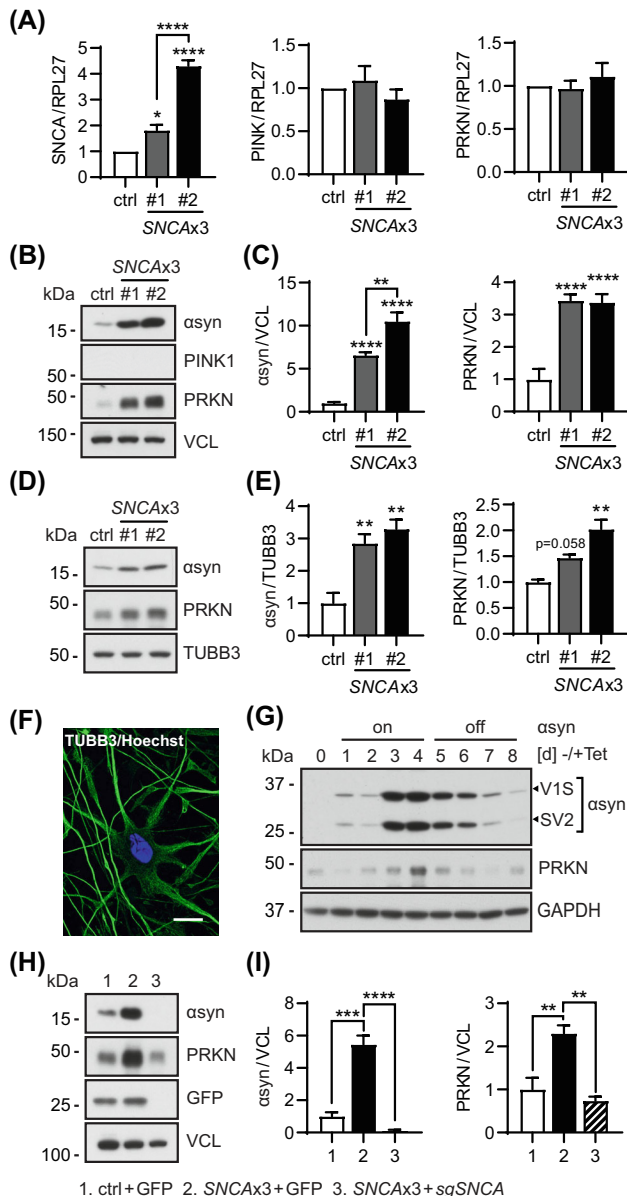


FIGURE 1 PRKN protein levels are consistently increased in cells with higher α syn expression. (A) Reverse transcriptase qPCR shows a significant increase of *SNCA* mRNA levels in both *SNCAx3* fibroblasts compared to a sibling control ($p = 0.016$ for #1 and $p < 0.0001$ for #2; $p < 0.0001$ for #1 vs. #2), while *PINK1* and *PRKN* mRNA levels remain unchanged among all three cell lines. $n = 4$ –5 independent experiments. (B) Representative western blot of control and two *SNCAx3* fibroblast lines. (C) Immunoblot quantification shows significantly increased protein levels of α syn ($p < 0.0001$ for both lines; $p = 0.0011$ for #1 vs. #2) and PRKN ($p < 0.0001$ for both lines) in two *SNCAx3* fibroblasts compared to control. $n = 6$ independent experiments. (D) Representative western blot of control and two *SNCAx3* iNeurons. (E) Immunoblot quantification shows significantly increased levels of α syn ($p = 0.0091$ for #1, $p = 0.0032$ for #2) and PRKN ($p = 0.058$ for #1, $p = 0.0016$ for #2) in two *SNCAx3* cells compared to control. Induction of the neuronal marker TUBB3 confirms the successful *trans*-differentiation of fibroblasts to iNeurons. $n = 3$ independent differentiation experiments. (F) Representative immunofluorescence images of iNeurons stained with TUBB3 (green) and Hoechst (blue) confirmed the neuronal conversion. Scale bar: 20 μ m. (G) Representative western blot of H4 cells shows an increase and then a decrease in PRKN protein when α syn expression was turned on (Tet $-$) for 4 days and then turned off (Tet $+$) for another 4 days. Tet, tetracycline. Note the H4 cell line is for bimolecular fluorescence complementation assays and expresses two split venus YFP tagged forms of α syn [Venus1- α syn (V1S) and α syn-Venus2 (SV2)] from a bidirectional promoter. (H) Representative western blot of fibroblasts transduced with GFP (ctrl + GFP and *SNCAx3* + GFP) and *SNCAx3* + sg*SNCA* are shown. (I) Western blot quantification shows significantly decreased α syn ($p < 0.0001$) and PRKN ($p = 0.0026$) levels in *SNCAx3* fibroblasts transduced with sg*SNCA* compared to the GFP control. $n = 3$ independent experiments. Quantifications are shown as fold change with the control set to 1. Data are shown as mean with standard error. One-way ANOVA, * $p < 0.05$, ** $p < 0.01$, *** $p < 0.001$, **** $p < 0.0001$ when compared to controls. Significance level between two groups as indicated by brackets.

compared to the sibling control (Figure 1B,C), consistent with their relative increase in mRNA. PINK1 protein was not detectable as expected in the absence of mitochondrial stress. However, PRKN protein levels were notably elevated in both triplication cell lines. A similar trend for elevated PRKN levels, though less pronounced, was observed when analyzing an additional, independent set of fibroblasts from a *SNC Ax2* carrier and the sibling control (Figure S1A,B).

To validate our observations in a different cell type, we directly converted the patient fibroblasts to iNeurons. Consistent to the fibroblast results, the relative increases of both α syn and PRKN proteins in the respective *SNC Ax3* compared to the control cells were maintained in iNeurons (Figure 1D,E). Successful neuronal conversion and morphology of the cells was confirmed by the expression of the neuronal marker TUBB3 in western blot and immunofluorescence staining (Figure 1D,F). To further corroborate our findings in an independent model, we employed a H4 neuroglioma cell line with a stable inducible expression system of split venus-tagged α syn [Venus1- α syn (V1S) and α syn-Venus2 (SV2)] [34]. Tetracycline was initially removed from the culture media to allow the expression of α syn for 4 days and was then added back in to shut off α syn transcription for another 4 days. Consistently, we found an increase of α syn protein upon induction followed by a decline over the second half of the time course (Figure 1G). Of note, PRKN protein levels followed a similar trend, gradually increasing over the first 4 days, peaking with the maximal expression of α syn, and then decreasing again over the last 4 days.

To confirm that elevated PRKN protein levels were indeed caused by the increased expression of α syn, we knocked-out α syn in the triplication fibroblasts using CRISPR/Cas9. Patient cells were transduced with a lentivirus expressing GFP as a control or a single guide RNA targeting the start codon of *SNCA* (*sgSNCA*). This strategy effectively abolished α syn expression from the triplication fibroblasts compared to the GFP control transduction (Figure 1H,I). Of note, elimination of α syn significantly reduced PRKN protein to levels seen in the control fibroblast line. Altogether, the analyses of different cell lines and rescue experiments highlight a close relationship between enhanced α syn and PRKN expression at the protein level.

3.2 | PRKN accumulation in *SNC Ax3* fibroblasts is linked to altered, basal autophagic flux

To explore possible mechanisms underlying PRKN protein accumulation in *SNC Ax3* fibroblasts, we first followed its half-life after protein synthesis inhibition via cycloheximide (CHX) treatment (Figure 2A,B). Typically, PRKN requires activation by PINK1 to release its auto-

inhibited conformation, but otherwise can be quite stable under basal, nonstress conditions. While no significant change in PRKN turnover rate was found in either of the three fibroblast lines over the duration of the treatment, slightly more PRKN protein was turned over after 48 h CHX treatment in the control fibroblast line when compared to each of the *SNC Ax3* fibroblasts (65% vs. 49% and 56%), suggesting a slightly slower degradation rate that may partially contribute to PRKN accumulation over time in the presence of elevated α syn expression.

In general, two major proteolytic pathways, the ubiquitin-proteasome and the autophagy-lysosome system, mediate cellular degradation, and α syn is known to interfere with both routes [43]. To explore the contribution of either, we first inhibited proteasome function in the control and *SNC Ax3* fibroblasts with epoxomicin (Epox) (Figure 2C). Successful proteasome inhibition was confirmed by the accumulation of CDKN1A after 24 h of treatment. However, no obvious change in PRKN levels was found in any of the three fibroblast lines. Next, we treated fibroblasts with the autophagy inhibitor bafilomycin A1 (Baf A1) (Figure 2D). Successful inhibition of autophagic flux was confirmed by a strong upregulation of LC3 across all lines, yet no additional increase of PRKN protein was noted. However, a significant increase in the LC3-II/I ratio in both *SNC Ax3* lines compared to the control was apparent at basal conditions, that is, in the absence of stress (Figure 2E). While this can be interpreted as either, an induction of autophagosome formation or a decrease in degradation rates, α syn has been previously linked to impairments of autophagic flux [19]. To ascertain this effect, we stimulated general autophagy in *SNC Ax3* fibroblasts by starvation. This led to a time-dependent decrease of PRKN protein to similar levels seen in the control fibroblast over a period of just 16 h (Figure 2F,G). Taken together, accumulation of PRKN protein in *SNC Ax3* fibroblasts was likely associated with an alteration of basal autophagy but could be effectively cleared and normalized by starvation-induced autophagy activation.

3.3 | Abnormally enhanced PRKN levels modify the mitophagy response in *SNC Ax3* fibroblasts

To assess potential functional consequences of the increased PRKN levels in cells, we next studied mitophagy upon acute mitochondrial stress. For this, fibroblasts were treated with mitochondrial stressor valinomycin (Val) and levels of PINK1 and PRKN as well as the mitophagy marker pS65-Ub and the PRKN substrate MFN2 were studied by western blot at different time points (Figure 3A,B). Induction of mitophagy led to an immediate and significant stabilization of PINK1 over time that was comparable across all three cell lines. In contrast, levels of the Ub ligase PRKN typically decrease over time once activated by PINK1. As expected, PRKN

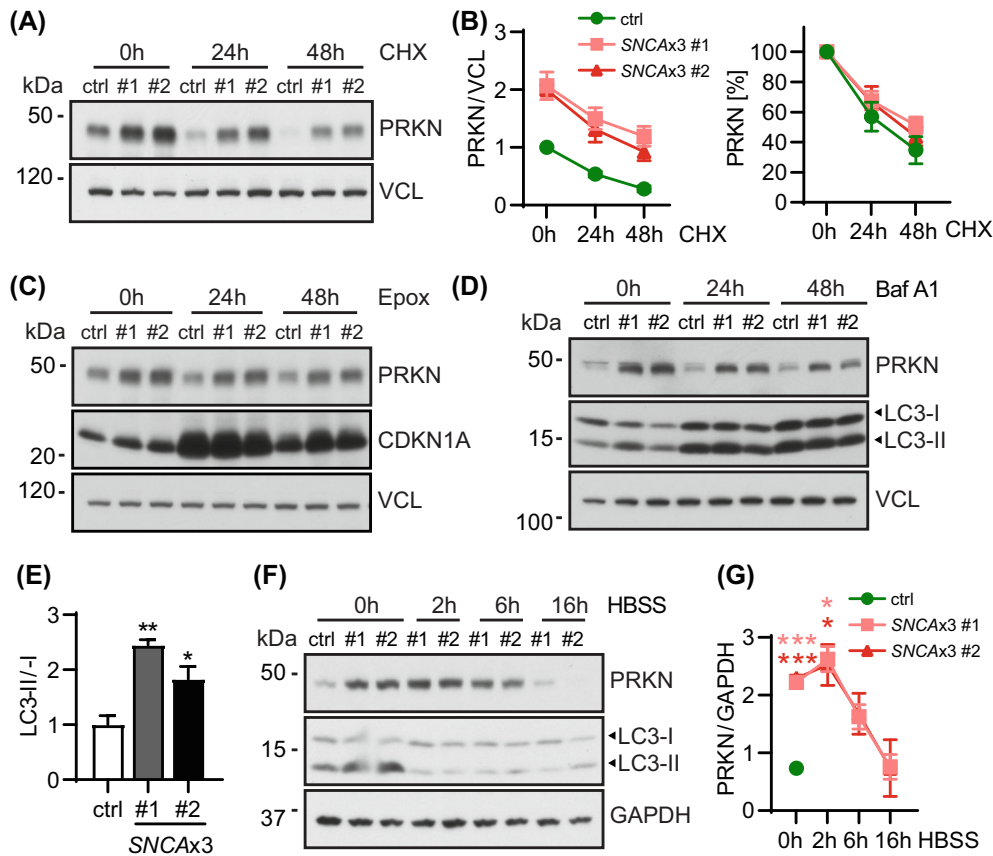


FIGURE 2 Activation of general autophagy reduces PRKN accumulation in *SNCAx3* fibroblasts. (A) Representative western blot of control and *SNCAx3* fibroblasts treated with cycloheximide (CHX) for the indicated timepoints. (B) Western blot quantification of PRKN normalized with the value of the control line set to 1 (left) or using each value at 0 h as 100% (right). Results show comparable PRKN turnover rates in all three fibroblast lines. $n = 4$ independent experiments. (C) Proteasome inhibition does not affect PRKN levels in control or *SNCAx3* fibroblasts. Representative western blot of PRKN, CDKN1A, and VCL from control and *SNCAx3* fibroblasts after 1 μ M epoxomicin (Epox) treatment for 0, 24, and 48 h. (D) Inhibition of autophagic flux does not further increase PRKN levels in *SNCAx3* fibroblasts. Representative western blot of PRKN, LC3, and VCL from control and *SNCAx3* fibroblasts after 200 nM bafilomycin A1 (Baf A1) treatment for 0, 24, and 48 h. (E) Immunoblot quantification shows significant increases of lipidated to unlipidated LC3 ratio (LC3-II/I) in two *SNCAx3* fibroblasts compared to control ($p = 0.0022$ for #1, $p = 0.031$ for #2). Quantifications are shown as fold change with the control set to 1. $n = 3$ independent experiments. (F) Representative western blot of control and *SNCAx3* fibroblasts treated by HBSS for indicated timepoints. (G) Western blot quantification shows that HBSS-induced autophagy activation is able to lower PRKN levels in *SNCAx3* fibroblasts to the control level after 16 h of starvation. $n = 2$ independent experiments. Data shown as mean with standard error. One-way ANOVA, * $p < 0.05$, ** $p < 0.01$, *** $p < 0.001$ in pink/red for the corresponding *SNCAx3* cells when compared to control at the same timepoint.

levels were significantly higher in both triplication lines, but the signal declined over time at a rate similar to the consanguineous control cells (data not shown). Yet, levels of the mitophagy tag pS65-Ub were also significantly elevated in the *SNCAx3* cells compared to the control. Consistently, Ub modification of MFN2 (MFN2-Ub) that is observed as a 8 kDa shifted band was also markedly increased in *SNCAx3* cells (especially at early time points). The significant boost of the pS65-Ub signal was additionally confirmed by immunofluorescence staining of fibroblasts followed by quantification with high content imaging (Figure 3C–E). Over time, both *SNCAx3* cells showed much greater accumulation of pS65-Ub-positive mitochondria than the control line. Similar findings were obtained from the *SNCAx2* fibroblasts that also showed elevated pS65-Ub levels

compared to the sibling control upon 24 h of Val treatment (Figure S1C).

Given that activated PRKN provides additional substrates for PINK1 and thereby typically amplifies the pS65-Ub response, we asked whether the abnormally increased levels of the E3 Ub ligase PRKN were causal to the elevated mitophagy signaling observed in *SNCAx3* fibroblasts. To test this hypothesis, we knocked down PRKN expression by siRNA to similar levels seen in the control fibroblast (Figure 4A,B). We then assessed mitophagy signaling again in response to Val treatment. While PINK1 stabilization over time remained similar, knockdown of PRKN reduced the pS65-Ub response to levels comparable to the control cell line. Taken together, our results suggest a primary role for elevated PRKN protein in exacerbating the pS65-Ub response in

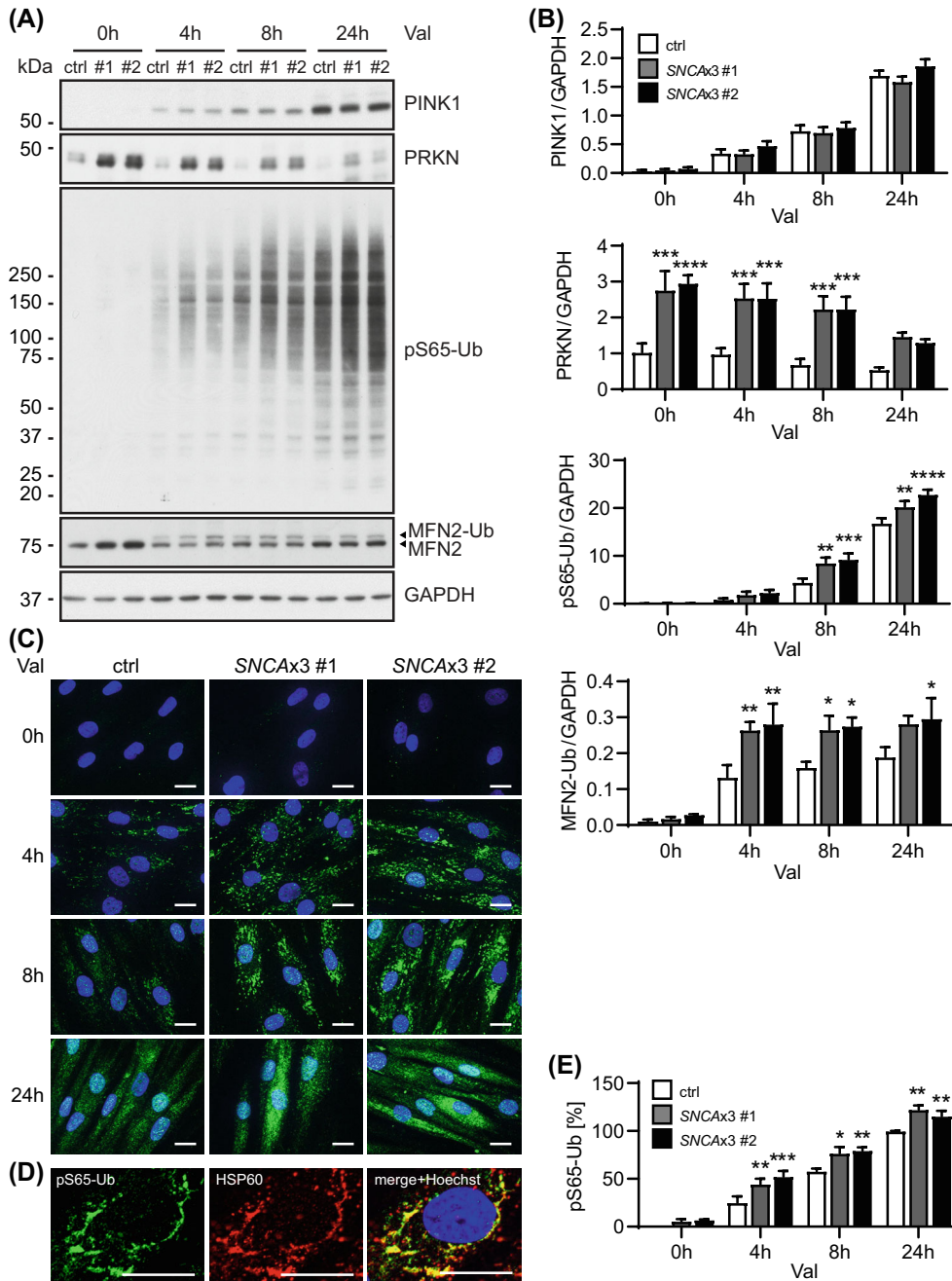


FIGURE 3 Increased mitophagy response upon acute stress in *SNCAx3* fibroblasts. (A) Representative western blot of control and two *SNCAx3* fibroblasts lines upon valinomycin (Val) treatment for the indicated time points. (B) Western blot quantification shows similar stabilization of PINK1, but significantly increased levels of PRKN, pS65-Ub, and ubiquitinated MFN2 (MFN2-Ub) in *SNCAx3* fibroblasts compared to the control with the same treatment (for PRKN, $p < 0.001$ for both lines at 0, 4, 8 h; for pS65-Ub, $p < 0.01$ for both lines at 8, 24 h; for MFN2-Ub, $p < 0.05$ for #1 at 4, 8 h and for #2 at 4, 8, and 24 h). $n = 6$ independent experiments. (C) Representative images of pS65-Ub immunofluorescence staining (green) in fibroblasts upon Val treatment. Scale bar: 20 μm .

(D) Representative immunofluorescence images of fibroblasts stained with pS65-Ub (green) and the mitochondrial marker HSP60 (red) showing colocalization of pS65-Ub on the mitochondria. Scale bar: 20 μm . (E) High content imaging quantification confirms the significant increase in pS65-Ub-positive signal in *SNCAx3* fibroblasts compared to the control with the same treatment ($p < 0.05$ for #1 and $p < 0.01$ for #2 at 4, 8, 24 h). $n = 4$ independent experiments. Data shown as mean with standard error. One-way ANOVA, * $p < 0.05$, ** $p < 0.01$, *** $p < 0.001$, **** $p < 0.0001$ when compared to the corresponding control at the same time point.

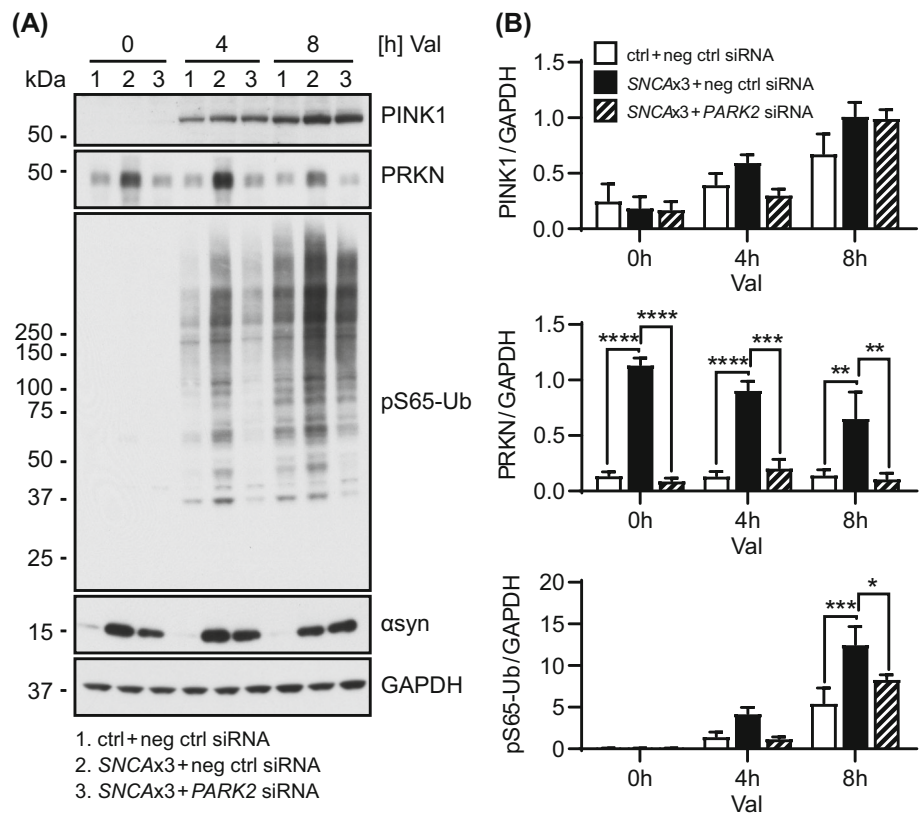
SNCAx3 fibroblasts. While PRKN protein seems to accumulate due to altered basal autophagy, the Ub ligase can be activated and its increased levels amplify the mitophagy response upon mitochondrial stress in *SNCAx3* fibroblasts.

3.4 | The mitophagy marker pS65-Ub correlates with the pathological αsyn load in LBD brain

To evaluate the disease relevance of findings from cell culture, we turned to human autopsy brain comparing

LBD cases with different burden of αsyn pathology to neurologically normal individuals. Given the lack of tools to reliably detect PINK1 and PRKN in tissue, we chose to focus on their joint product pS65-Ub to assess mitophagy alterations by immunohistochemistry [31, 33, 44]. Compared to our previous work, here we examined pS65-Ub levels in LBD cases with *SNCA* mutations or multiplications (LBD^{mut} group) that generally show more severe αsyn pathology at younger age [45, 46]. Age- and sex-matched neurologically normal controls and sporadic LBD cases (LBD group) were also included in the analysis. For a summary and the detailed characteristics of all subjects studied, see Tables S2 and S3, respectively.

FIGURE 4 PRKN knockdown in *SNCAx3* fibroblasts normalizes the mitophagy response. (A) Representative western blot of control and *SNCAx3* fibroblasts transfected with negative control siRNA (ctrl + neg ctrl siRNA and *SNCAx3* + neg ctrl siRNA) and *SNCAx3* fibroblasts transfected with *PARK2* siRNA (*SNCAx3* + *PARK2* siRNA). (B) Western blot quantification shows that PRKN knockdown in *SNCAx3* fibroblasts significantly reduces PRKN ($p < 0.01$ at 0, 4, 8 h) and pS65-Ub ($p = 0.019$ at 8 h) levels but does not affect PINK1 and α syn levels when compared to negative control siRNA transfected *SNCAx3* fibroblasts with same duration of valinomycin (Val) treatment. $n = 3$ independent experiments. Data shown as mean with standard error. One-way ANOVA, * $p < 0.05$, ** $p < 0.01$, *** $p < 0.001$, **** $p < 0.0001$.



Significant pathological burden, as determined by α syn (NACP) immunostaining, was detected in the substantia nigra (SN) and hippocampus (Figure S2A) as well as in the amygdala, nucleus basalis of Meynert (nbM), and putamen (Figure 5A,B).

As expected, the *LBD^{mut}* group showed more widespread and more severe α syn pathology compared to the *LBD* group in most of the regions examined. In line with these and our prior findings [31], significant increases of the pS65-Ub were restricted to the SN and hippocampus in the *LBD* cases (Figure S2B) but were observed in all studied brain regions in the *LBD^{mut}* group (Figure 5C,D). The increased pS65-Ub level was particularly prominent in the *SNCA* triplication case compared to *SNCA* duplication or *A53T* mutation cases, in agreement with their respective α syn burden. The increase of pS65-Ub was independent of the comorbid tau pathology as there was no significant difference in the density of CP13 (phospho-tau) positive cells between *LBD* and *LBD^{mut}* groups (Figures S2C and S3). However, pS65-Ub significantly correlated with an increased burden of neuropathological α syn across all brain regions studied (Figure 5E). To further validate this finding, we immunostained and quantified pS65-Ub in a mouse model overexpressing wild-type human α syn (Line D) [38]. Transgenic mice expressing high levels of human α syn showed significant increases of pS65-Ub immunoreactive signal in the brain compared to the respective non-transgenic controls (Figure S4). Consistent with results from human brain, pS65-Ub levels also significantly

correlated with the α syn burden in brains of transgenic mice (Figure 5F).

3.5 | pS65-Ub accumulates early on during the development of and in proximity to the α syn pathology

To investigate the spatial relationship between mitophagy changes and α syn pathology, we immunostained human tissue for pS65-Ub and phosphorylated- α syn (pS129- α syn), the pathognomonic form of α syn, and used super-resolution microscopy for colocalization studies (Figure 6A). We first categorized pS65-Ub-positive cells in the SN based on their respective pS129- α syn immunoreactivity: no pS129- α syn, diffuse pS129- α syn, or aggregated pS129- α syn staining. While only a small percentage of pS65-Ub-positive cells were completely devoid of pS129- α syn immunoreactivity, their number was slightly greater in the *LBD^{mut}* cases compared to *LBD* cases (Figure 6B). The *LBD^{mut}* group also contained more pS65-Ub-positive cells with diffuse pS129- α syn staining particularly in the *SNCA* triplication case (the highest data point). The number of pS65-Ub positive cells with aggregated pS129- α syn in the form of either cortical-type or classical, brainstem-type LBs were rather similar between both disease groups. In either case, the majority of pS65-Ub positive structures did not necessarily colocalize with the pS129- α syn signal but were especially abundant in cells with smaller, pathological α syn aggregates

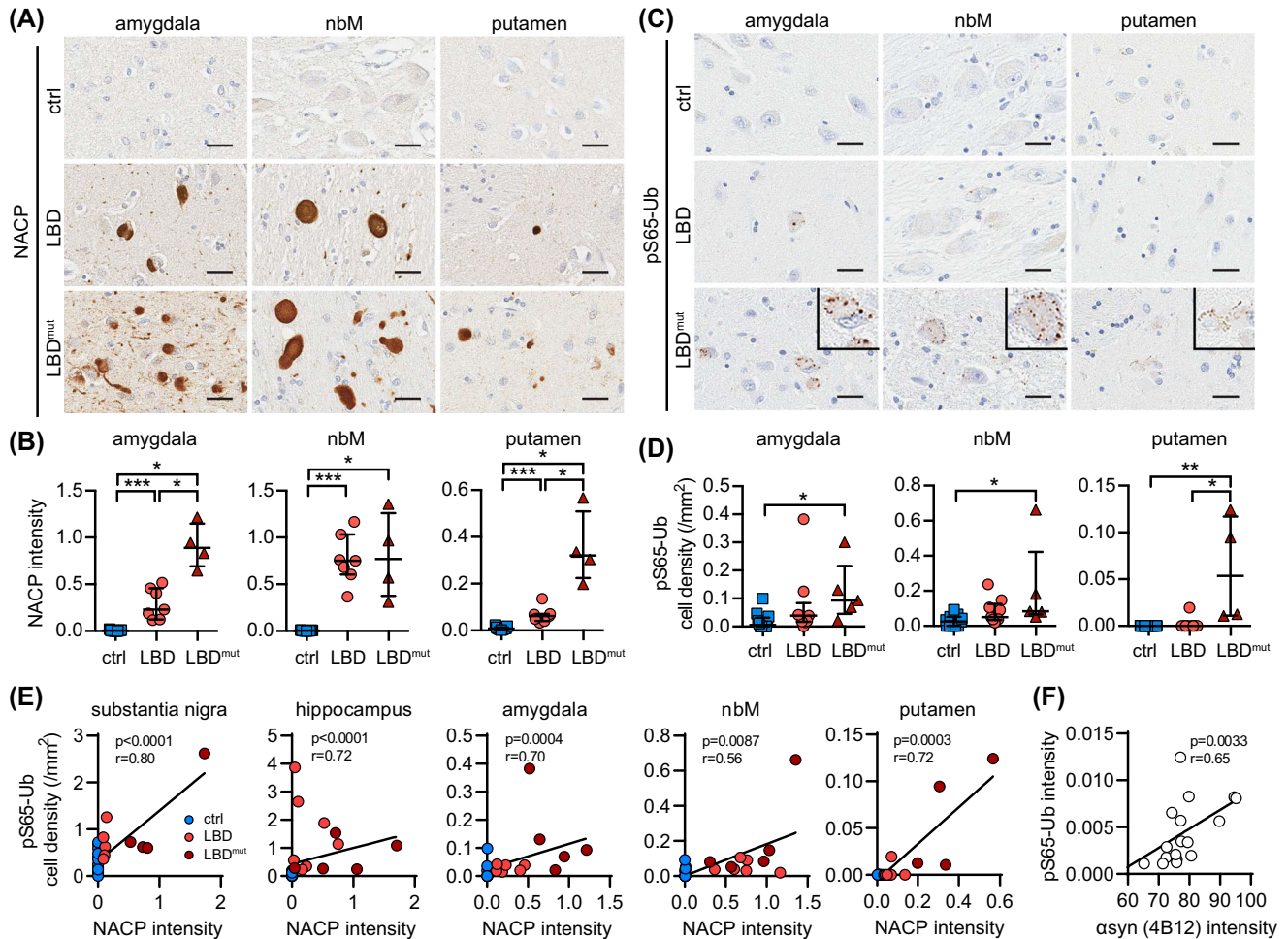


FIGURE 5 The mitophagy marker pS65-Ub is increased across regions in human autopsy LBD brains with *SNCA* missense mutations or multiplications. Representative images of (A) α syn (stained by NACP) and (C) pS65-Ub immunostaining in the indicated brain regions from control, LBD, and LBD^{mut} groups. Insets show magnified views of pS65-Ub positive cells in all three regions. Scale bar: 25 μ m. (B) NACP intensity is significantly increased in LBD and increased further in the LBD^{mut} group in the amygdala, nbM, and putamen compared to the age-matched controls ($p < 0.0001$ for LBD, $p = 0.0015$ for LBD^{mut}, $p = 0.0061$ for LBD vs. LBD^{mut}). (D) pS65-Ub-positive cell density is significantly increased only in the LBD^{mut} group in the amygdala ($p = 0.004$), nbM ($p = 0.0053$), and putamen ($p = 0.0005$) compared to age-matched controls. Kruskal–Wallis and Mann–Whitney U tests followed by adjustment with Bonferroni correction, $*p < 0.0167$ (i.e., the statistical significance threshold after Bonferroni correction), $**p < 0.001$, $***p < 0.0001$. Data is shown as median with interquartile range. (E) pS65-Ub positive cell density and NACP intensity are strongly correlated in the substantia nigra, hippocampus, amygdala, nbM, and putamen. Spearman’s test of correlation, significance threshold: $p < 0.01$. $n = 11$ – 15 for controls, $n = 6$ – 9 for LBD group, $n = 4$ – 5 for LBD^{mut} group. nbM, nucleus basalis of Meynert. (F) pS65-Ub and human α syn levels are strongly correlated in brains of Line D mice. Spearman’s test of correlation, significance threshold: $p < 0.05$. $n = 18$.

(Figure 6C). pS65-Ub positive puncta were frequently found adjacent to or closely decorated the surface of α syn aggregates that resembled premature LBs in neurons in the studied regions (Figure 6D). However, in neurons with rather mature LBs, pS65-Ub granules were less prominent, suggesting that mitophagy changes occur early on but may not be detectable during late-stage pathology.

3.6 | pS65-Ub accumulates alongside neuropathological α syn in LBD, but not in MSA brain

LBD and MSA are both synucleinopathies but are pathologically characterized by distinct intracellular α syn

inclusions, namely LB-type deposits and glial cytoplasmic inclusions (GCIs), respectively [3, 47]. To explore the effect of different α syn inclusions on mitophagy, we examined α syn burden and compared pS65-Ub levels in brains of LBD and MSA patients along with their age- and sex-matched neurologically normal controls. We chose to examine the amygdala, nbM, and putamen here to cover brain regions with low, intermediate, or high α syn burden in both types of diseases (Figure 7A). While both LBD and LBD^{mut} groups contained high α syn burden in the amygdala, α syn levels in LBD^{mut} cases in this region were similar to α syn levels in MSA cases in the putamen and thus this group was used here for comparison with MSA. α syn (NACP) immunostaining confirmed the strongest α syn burden in the amygdala in LBD^{mut}

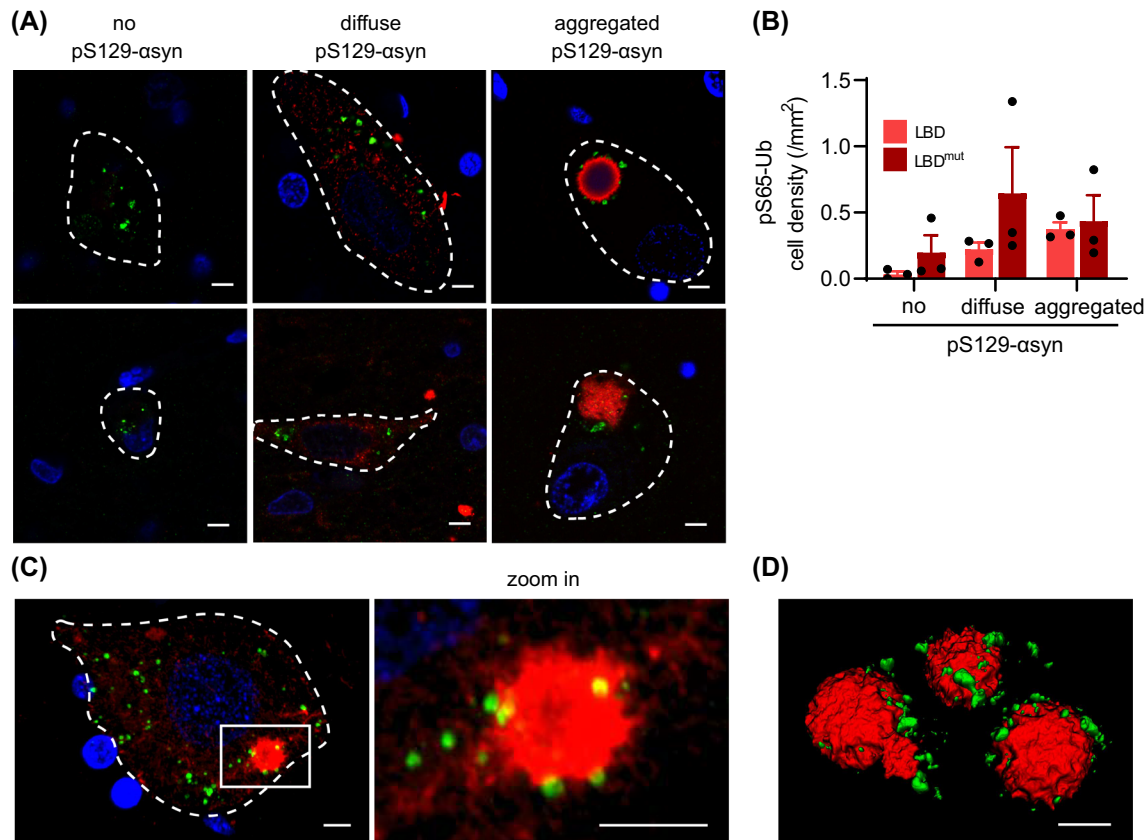


FIGURE 6 Spatial relationship between pS65-Ub and α syn pathology in LBD. (A) Representative images of pS65-Ub positive cells with different pS129- α syn immunoreactive signals. Classical (top right image) and cortical (bottom right image) LBs with double immunostaining of pS65-Ub (green) and pS129- α syn (red) are shown. (B) The quantification of pS65-Ub-positive cell density that was categorized based on their respective pS129- α syn immunoreactivity in the substantia nigra of three LBD and three LBD^{mut} cases. (C) Representative immunofluorescence images in 3D maximum projection rendering of one cell containing small pS129- α syn-positive aggregation is shown. A magnified image of the boxed area is shown to the right. pS65-Ub-positive granules (green) surround the pS129- α syn-positive aggregation (red). (D) The spatial relationship of pS65-Ub- and pS129- α syn-positive LB is shown in 3D surface rendering.

and in the putamen in MSA with comparable levels seen in the nbM in both diseases (Figure 7B,C). pS65-Ub seemed to track exclusively with the LB pathology found in LBD^{mut} as levels of pS65-Ub were also the highest in the amygdala, somewhat decreased in the nbM, and the lowest in the putamen (Figure 7D). On the contrary, pS65-Ub signals were not elevated in MSA cases compared to controls, even in the nbM or the putamen with higher α syn burden and despite the additional tau pathology (Figure 7E).

Collectively our new data confirm and extend previous findings to additional brain regions from overall younger, but more severe cases of LBD that show more advanced and more widespread neuropathology. In subjects with disease-causing missense mutations or multiplications of *SNCA*, pS65-Ub levels were significantly increased and strongly correlated with the α syn pathology in all regions analyzed and independently of the comorbid tau pathology. We further discovered that despite comparable neuropathological load, the observed mitophagy alterations were specific to LB-type deposits of α syn rather than GCIs seen in MSA.

4 | DISCUSSION

Characterization of primary fibroblasts obtained from siblings with or without *SNCA* triplications showed that PRKN protein levels increase in cells with higher α syn expression. We confirmed this effect in independent sets of patients' cells and different cell types including directly differentiated neurons and an inducible α syn overexpression model. Moreover, *SNCA* knockout by CRISPR/Cas9 caused a reduction of PRKN protein to control levels. PINK1 and PRKN mRNA however remained unchanged, arguing for a posttranslational mechanism rather than a compensatory transcriptional effect. While α syn has been proposed to impair mitochondrial function directly or indirectly through a plethora of mechanisms [25–28, 48–51], we could not observe stabilization of PINK1 protein in *SNCAx3* cells as one would expect if increased expression of α syn caused mitochondrial damage. Likewise, at baseline we did not detect an increase of pS65-Ub, the most sensitive readout for activation of the PINK1-PRKN pathway. Instead, we found elevated levels of α syn to be associated with an altered basal

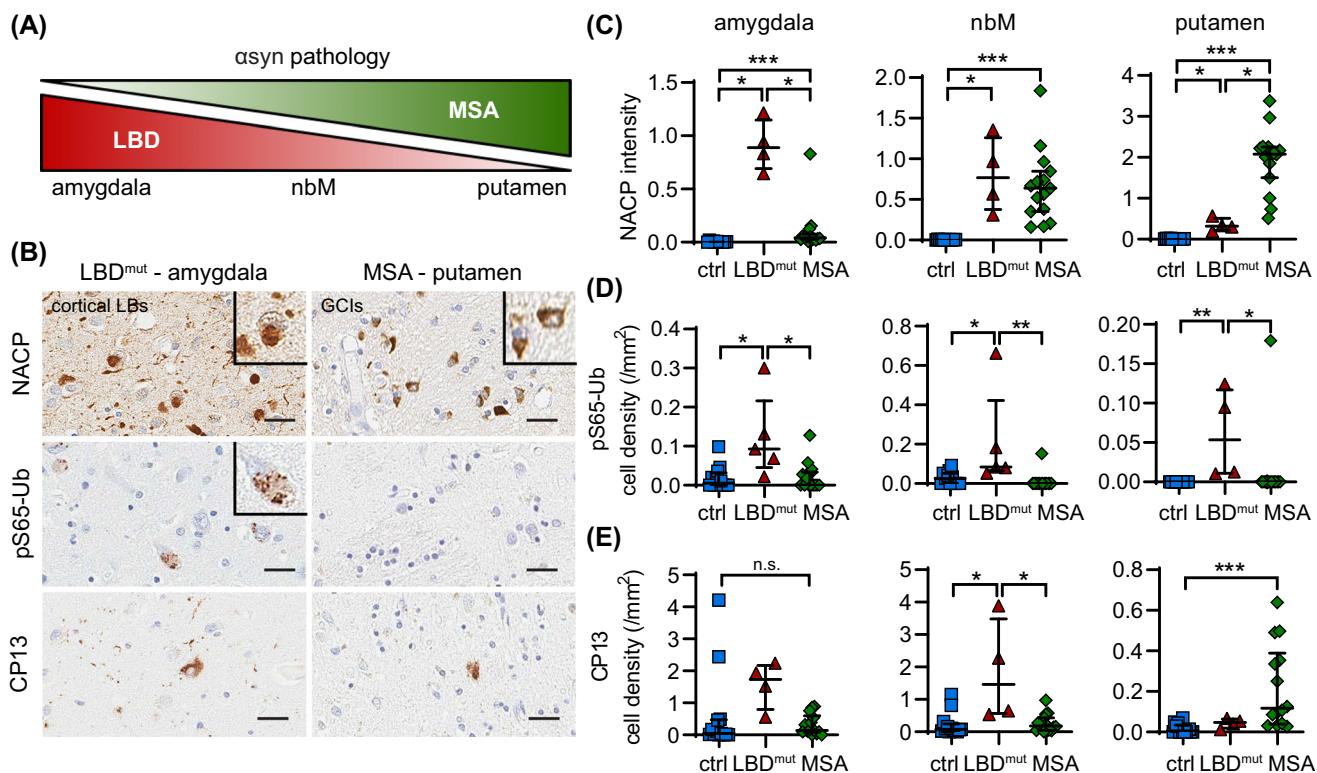


FIGURE 7 The increase of the mitophagy marker pS65-Ub in human autopsy brain is associated with LB-, but not GCI-type of α syn pathology. (A) The schematic shows that α syn pathology is predominantly found in the amygdala and to a lesser extent in the nbM and putamen in LBD, while it is predominantly found in the putamen and to a lesser extent in the amygdala and nbM in MSA. (B) Representative images of α syn (NACP, top), pS65-Ub (middle), and phospho-tau (CP13, bottom) immunostaining in the amygdala and putamen of LBD^{mut} and MSA cases, respectively. Scale bar: 25 μ m. Insets show magnified views of cortical type LBs in LBD, GCIs in MSA, and pS65-Ub positive cells. (C) Consistent with the schematic, NACP intensity is differentially increased in the amygdala, nbM, and putamen of LBD^{mut} and MSA cases compared to age-matched controls ($p = 0.0015$ for LBD^{mut}, $p < 0.0001$ for MSA, $p < 0.01$ for LBD^{mut} vs. MSA). (D) pS65-Ub positive cell density is increased in all three regions, but only in the LBD^{mut} group compared to age-matched controls ($p = 0.004$, 0.0053 , and 0.0005 in the amygdala, nbM, and putamen, respectively) and MSA group ($p = 0.0035$, 0.0003 , and 0.0013 in the amygdala, nbM, and putamen, respectively). (E) CP13 positive cell density is selectively increased in the nbM of the LBD^{mut} group ($p = 0.0097$ for LBD^{mut}, $p = 0.0062$ for LBD^{mut} vs. MSA) and in the putamen of MSA cases ($p < 0.0001$) compared to age-matched controls. $n = 11$ – 15 for controls, $n = 4$ – 5 for LBD^{mut} group, $n = 14$ – 15 for MSA group. Kruskal–Wallis and Mann–Whitney U tests followed by adjustment with Bonferroni correction, $*p < 0.0167$ (i.e., the statistical significance threshold after Bonferroni correction), $**p < 0.001$, $***p < 0.0001$, n.s., not significant. Data is shown as median with interquartile range. GCI, glial cytoplasmic inclusion; LB, Lewy body; nbM, nucleus basalis of Meynert.

autophagy, which likely contributed to the accumulation of PRKN protein.

The impairment of autophagy through mutant or aggregated α syn is well documented in the literature (reviewed in [6]), but our current study suggests that even increased levels of soluble α syn can alter basal autophagic flux. While these effects were subtle and largely reversible in fibroblasts, increased soluble α syn was recently identified as a shared feature of induced pluripotent stem cells (iPSC)-derived dopamine neurons from young-onset PD patients [52]. The mechanism(s) by which soluble α syn can alter basal flux are unresolved, but may include both direct and indirect effects on autophagy or lysosomes that are probably also context dependent with regard to cell type and actual α syn species. Regardless, stalled basal autophagy may not only contribute to spreading and propagation of α syn, but partial degradation can lead to further aberrant processing of

α syn which may produce forms that are even more aggregation-prone and neurotoxic [28, 53–55]. The resulting pathologic α syn species then preferentially bind to and impair mitochondria and contribute to a viscous cycle that directly affects the PINK1-PRKN-mediated mitophagy [27, 28, 49–51, 56, 57].

We hypothesize that PRKN most likely accumulates in its auto-inhibited form as PINK1-dependent recruitment and activation results in its own degradation alongside damaged mitochondria. Consistently, PRKN protein accrues in PINK1 knockout cells and tissue due to lack of prerequisite activation (Watzlawik et al., in submission). Notwithstanding, the increased pool of PRKN in *SNCx3* fibroblasts was activatable and, due to the known feed-forward loop in which products of PRKN become additional substrates for PINK1 [8], strongly amplified the pS65-Ub response to acute mitochondrial insult. A boosted pS65-Ub signal may lead to

additional buildup of mitophagosomes or, in case of sufficient degradative capacities, to excessive mitophagy, both of which have been described in the context of α syn overexpression [25, 26, 48]. Yet, levels of the E3 Ub ligase PRKN, once activated, eventually declined at similar rates in control and *SNCAx3* fibroblasts, suggesting a comparable turnover of damaged mitochondria among three fibroblast lines. Although pharmacological block of neither autophagy nor proteasome system alone further increased levels of PRKN, induction of general autophagy by nutrient starvation in *SNCAx3* cells effectively cleared the elevated pool of PRKN over time.

In human LBD autopsy brain, we previously identified an age-dependent increase of the mitophagy marker pS65-Ub as well as independent α syn- and tau-mediated associations in select vulnerable brain regions including the SN and the hippocampus [31, 33]. Compared to these prior studies, we here expanded our analyses to younger and more severe cases of LBD including individuals with *SNCA* missense mutations or gene multiplications (LBD^{mut} group). We observed significant increases of pS65-Ub in all brain regions analyzed, including amygdala, nbM, and putamen, areas that are typically affected later than the SN or in more aggressive forms of LBD. Since tau can independently drive pS65-Ub in both human brain and transgenic mice [44], we adjusted for the comorbid phospho-tau pathology and identified a strong correlation of pS65-Ub with the more abundant α syn pathology. Consistently, pS65-Ub also strongly correlated with α syn levels in a transgenic mouse model overexpressing human α syn in neurons [38]. However, comparison of LBD to MSA revealed a significant pS65-Ub increase only in the context of LBs, but not GCIs, despite a similar or higher burden of pathologic α syn in vulnerable regions, and regardless of greater neuronal loss seen in some, but not all MSA cases. While it is known that pathological α syn from LBs and GCIs is conformationally and biologically distinct [58–60], it remains unclear whether our findings primarily reflect a cell type specific mitophagy effect (neurons vs. oligodendrocytes), a difference in the respective α syn aggregate, or the diverse structures and other molecular content of the inclusions.

While loss of PINK1 or PRKN causes EOPD and impedes the initial steps of mitophagy, that is, the identification and labeling of damaged mitochondria with pS65-Ub, the age-dependent decline in degradative capacities may impair the pathway at later steps contributing to sporadic late-onset PD. However, loss of PINK1 or PRKN not only results in the accumulation of dysfunctional mitochondria, but also contributes to α syn aggregation in various cell and animal models [10, 61–64]. Thus, a functional relationship and convergence of both α syn and PINK1-PRKN-mediated mitophagy is further emerging [9]. In line with our previous study [31], the results herein suggest that mitophagy alterations in LBD brain may happen early on and prior to prominent

α syn aggregation and maturation into LBs. Such overarching concept is also compatible with the earlier notion that PRKN activity might be required for LB formation, in part because mutant cases seem to mostly lack LBs [65–68] as well as more recent findings that clusters of membranous compartments derived from mitochondria and lysosomes accumulate in LBs [30, 69]. Furthermore, it was suggested that the process of LB formation may be the consequence of dysfunctions in either of these organelles [29], and the major driver of neurodegeneration [70, 71].

With the ongoing discussion about the biological origin of synucleinopathies and what triggers the disease relevant events [72, 73], our study further emphasizes the need to determine the specific bioactivity of the various forms of α syn. We found similar outcomes associated with higher levels of α syn in cells and in brain tissue (i.e., higher levels of the mitophagy tag pS65-Ub), but the underlying mechanisms might be distinct. Although pS65-Ub is a direct readout of both PINK1 and PRKN enzymatic activities as well as a quantitative measure of mitochondrial damage, both increased activation of mitophagy as well as reduced flux through the autophagy-lysosome system can lead to pS65-Ub accumulation. The current detailed analyses in human brain tissue mostly focused on LBs and not on GCIs. Going forward, additional analyses in iPSC-derived cultures, in novel organoid models [74], and in in vivo animal models are needed to confirm our findings in LBs vs. GCIs and to further dissect effects of individual α syn species on different organelles and aspects involved in mitophagy. High resolution imaging of fixed tissue should help to at least approximate the most likely primary defects leading to the increase in pS65-Ub [44]. Yet, this seems to strongly depend on the respective brain region and cell type as well as the nature and progression of the neuropathology. Nevertheless, our current findings together with the identification of pS65-Ub in patients' biofluids [75] may help facilitate a differential diagnosis between synucleinopathies despite the similar extrapyramidal symptoms seen in PD and MSA.

AUTHOR CONTRIBUTIONS

Conceptualization: Wolfdieter Springer, Xu Hou. *Methodology:* Xu Hou, Fabienne C. Fiesel. *Formal analysis:* Xu Hou. *Investigation:* Xu Hou, Taylor Hsuan-Yu Chen, Jenny M. Bredenberg, Shunsuke Koga. *Resources:* Shunsuke Koga, Ayman H. Faroqi, Marion Delenclos, Guojun Bu, Zbigniew K. Wszolek, Jonathan A. Carr, Owen A. Ross, Pamela J. McLean, Melissa E. Murray, Dennis W. Dickson. *Writing—original draft:* Xu Hou, Wolfdieter Springer. *Visualization:* Xu Hou. *Funding acquisition:* Wolfdieter Springer.

ACKNOWLEDGMENTS

We are grateful to the patients and their families who made this study possible. We thank Monica Castanedes-

Casey and Virginia R. Phillips from the Neuropathology Laboratory for processing human postmortem tissues and the excellent technical support. We thank the Center for Regenerative Medicine and the Neuroregeneration Laboratory for biobanking of patient cells at Mayo Clinic Florida. We thank Audrey J. Strongosky for coordinating clinical research studies and help with obtaining patient specimens. We also thank the late Dr. Peter Davies from the Feinstein Institute for his generous contribution of CP13 antibodies.

FUNDING INFORMATION

W.S., O.A.R., P.J.M., and D.W.D. are members of the American Parkinson Disease Association (APDA) Center for Advanced Research at Mayo Clinic Florida and are further supported by the National Institute of Neurological Disorders and Stroke (NIH/NINDS) Lewy Body Dementia Center Without Walls (U54 NS110435). W.S. is additionally supported by NIH (R01 NS085070, R01 NS110085, and R56 AG062556), the Department of Defense Congressionally Directed Medical Research Programs (CDMRP) (W81XWH-17-1-0248), the Michael J. Fox Foundation for Parkinson's Research (MJFF), the Ted Nash Long Life Foundation, Mayo Clinic Foundation, the Center for Biomedical Discovery (CBD), and the Robert and Arlene Kogod Center on Aging. X.H. is supported by a pilot grant and a developmental project award from the Mayo Clinic Alzheimer Disease Research Center (ADRC, P30 AG062677) and fellowships awarded by the APDA and Alzheimer's Association (AARF-22-973152). F.C.F. is the recipient of fellowships from the Younkin Scholar Program and the APDA and is supported in part by the Florida Department of Health—Ed and Ethel Moore Alzheimer's Disease Research Program (22A07), the MJFF, a Gerstner Family Career Development Award from the Center for Individualized Medicine (CIM) and an auxiliary award from the CBD at Mayo Clinic. Z.K.W. is partially supported by the NIH (U19 AG063911), Mayo Clinic Center for Regenerative Medicine, gifts from the Donald G. and Jodi P. Heeringa Family, the Haworth Family Professorship in Neurodegenerative Diseases fund, and the Albertson Parkinson's Research Foundation. A.H.F., M.D., P.J.M. are partially supported by Mayo Clinic APDA Center for Advanced Research grant and American Brain Foundation (ABF) Cure One Cure All grant. O.A.R. is supported in part by NIH (P50 NS072187, R01 NS078086, U54 NS100693), Department of Defense (W81XWH-17-1-0249), the ABF, the MJFF, the Little Family Foundation, and the CIM at Mayo Clinic. D.W.D. is further supported by the Mangurian Foundation Lewy Body Dementia Program at Mayo Clinic.

CONFLICT OF INTEREST STATEMENT

Mayo Clinic, F.C.F., and W.S. have filed a patent related to PRKN activators. Z.K.W. serves as an external advisory board member for Vigil Neuroscience, Inc.

Additional funding sources to disclose but not pertinent to the current study include grants from Biohaven Pharmaceuticals, Inc. (BHV4157-206 and BHV3241-301 to Z.K.W.), Neuraly, Inc. (NLY01-PD-1 to Z.K.W.), Vigil Neuroscience, Inc. (VGL101-01.001 and VGL101-01.002 to Z.K.W.), and Amazentis SA (to W.S.). All other authors declare they have no competing interests. This research was conducted in compliance with Mayo Clinic conflict of interest policies.

DATA AVAILABILITY STATEMENT

The datasets used and/or analyzed during the current study available from the corresponding author on reasonable request.

ETHICS STATEMENT

The collection, processing, and analyses of primary dermal fibroblast were approved by the Institutional Review Board at Mayo Clinic. All procedures involving animals were in accordance with the ethical standards and approved by the Institutional Animal Care and Use Committee at Mayo Clinic. All brain samples are from autopsies performed after approval by the legal next-of-kin. Research on de-identified postmortem brain tissue is considered exempt from human subjects' regulations by the Mayo Clinic Institutional Review Board.

ORCID

Xu Hou  <https://orcid.org/0000-0003-3011-4378>

Shunsuke Koga  <https://orcid.org/0000-0001-8868-9700>

REFERENCES

1. Lees AJ, Hardy J, Revesz T. Parkinson's disease. *Lancet*. 2009; 373:2055–66.
2. Dickson DW, Braak H, Duda JE, Duyckaerts C, Gasser T, Halliday GM, et al. Neuropathological assessment of Parkinson's disease: refining the diagnostic criteria. *Lancet Neurol*. 2009;8: 1150–7.
3. McCann H, Stevens CH, Cartwright H, Halliday GM. Alpha-synucleinopathy phenotypes. *Parkinsonism Relat Disord*. 2014;20: (Suppl 1):S62–7.
4. Esteves AR, Arduino DM, Silva DF, Oliveira CR, Cardoso SM. Mitochondrial dysfunction: the road to alpha-synuclein oligomerization in PD. *Parkinsons Dis*. 2011;2011:693761.
5. Monzio Compagnoni G, Di Fonzo A. Understanding the pathogenesis of multiple system atrophy: state of the art and future perspectives. *Acta Neuropathol Commun*. 2019;7:113.
6. Hou X, Watzlawik JO, Fiesel FC, Springer W. Autophagy in Parkinson's disease. *J Mol Biol*. 2020;432:2651–72.
7. Moors T, Paciotti S, Chiasserini D, Calabresi P, Parnetti L, Beccari T, et al. Lysosomal dysfunction and alpha-synuclein aggregation in Parkinson's disease: diagnostic links. *Mov Disord*. 2016;31:791–801.
8. Truban D, Hou X, Caulfield TR, Fiesel FC, Springer W. PINK1, parkin, and mitochondrial quality control: what can we learn about Parkinson's disease pathobiology? *J Parkinsons Dis*. 2017;7: 13–29.
9. Ryan BJ, Hoek S, Fon EA, Wade-Martins R. Mitochondrial dysfunction and mitophagy in Parkinson's: from familial to sporadic disease. *Trends Biochem Sci*. 2015;40:200–10.
10. Gisbert S, Brehm N, Weil J, Seidel K, Rub U, Kern B, et al. Potentiation of neurotoxicity in double-mutant mice with Pink1

- ablation and A53T-SNCA overexpression. *Hum Mol Genet.* 2015; 24:1061–76.
11. Stichel CC, Zhu XR, Bader V, Linnartz B, Schmidt S, Lubbert H. Mono- and double-mutant mouse models of Parkinson's disease display severe mitochondrial damage. *Hum Mol Genet.* 2007;16: 2377–93.
 12. Creed RB, Goldberg MS. Analysis of alpha-synuclein pathology in PINK1 knockout rat brains. *Front Neurosci.* 2018;12:1034.
 13. Creed RB, Goldberg MS. Enhanced susceptibility of PINK1 knockout rats to alpha-synuclein fibrils. *Neuroscience.* 2020;437: 64–75.
 14. Todd AM, Staveley BE. Pink1 suppresses alpha-synuclein-induced phenotypes in a drosophila model of Parkinson's disease. *Genome.* 2008;51:1040–6.
 15. Yasuda T, Miyachi S, Kitagawa R, Wada K, Nihira T, Ren YR, et al. Neuronal specificity of alpha-synuclein toxicity and effect of parkin co-expression in primates. *Neuroscience.* 2007;144:743–53.
 16. Lo Bianco C, Schneider BL, Bauer M, Sajadi A, Brice A, Iwatsubo T, et al. Lentiviral vector delivery of parkin prevents dopaminergic degeneration in an alpha-synuclein rat model of Parkinson's disease. *Proc Natl Acad Sci U S A.* 2004;101:17510–5.
 17. Krzystek TJ, Banerjee R, Thurston L, Huang J, Swinter K, Rahman SN, et al. Differential mitochondrial roles for alpha-synuclein in DRP1-dependent fission and PINK1/parkin-mediated oxidation. *Cell Death Dis.* 2021;12:796.
 18. Chung E, Choi Y, Park J, Nah W, Park J, Jung Y, et al. Intracellular delivery of parkin rescues neurons from accumulation of damaged mitochondria and pathological alpha-synuclein. *Sci Adv.* 2020;6:eaba1193.
 19. Xilouri M, Brekk OR, Stefanis L. Autophagy and alpha-synuclein: relevance to Parkinson's disease and related synucleopathies. *Mov Disord.* 2016;31:178–92.
 20. Ordonez DG, Lee MK, Feany MB. Alpha-synuclein induces mitochondrial dysfunction through Spectrin and the Actin cytoskeleton. *Neuron.* 2018;97:108–124.e106.
 21. Bido S, Soria FN, Fan RZ, Bezaud E, Tieu K. Mitochondrial division inhibitor-1 is neuroprotective in the A53T-alpha-synuclein rat model of Parkinson's disease. *Sci Rep.* 2017;7:7495.
 22. Paillusson S, Gomez-Suaga P, Stoica R, Little D, Gissen P, Devine MJ, et al. Alpha-synuclein binds to the ER-mitochondria tethering protein VAPB to disrupt Ca(2+) homeostasis and mitochondrial ATP production. *Acta Neuropathol.* 2017;134:129–49.
 23. Choi ML, Chappard A, Singh BP, Maclachlan C, Rodrigues M, Fedotova EI, et al. Pathological structural conversion of alpha-synuclein at the mitochondria induces neuronal toxicity. *Nat Neurosci.* 2022;25:1134–48.
 24. Creed RB, Memon AA, Komaragiri SP, Barodia SK, Goldberg MS. Analysis of hemisphere-dependent effects of unilateral intrastratial injection of alpha-synuclein pre-formed fibrils on mitochondrial protein levels, dynamics, and function. *Acta Neuropathol Commun.* 2022;10:78.
 25. Choubey V, Safiulina D, Vaarmann A, Cagalinec M, Wareski P, Kuum M, et al. Mutant A53T alpha-synuclein induces neuronal death by increasing mitochondrial autophagy. *J Biol Chem.* 2011; 286:10814–24.
 26. Chen L, Xie Z, Turkson S, Zhuang X. A53T human alpha-synuclein overexpression in transgenic mice induces pervasive mitochondria macroautophagy defects preceding dopamine neuron degeneration. *J Neurosci.* 2015;35:890–905.
 27. Di Maio R, Barrett PJ, Hoffman EK, Barrett CW, Zharikov A, Borah A, et al. Alpha-synuclein binds to TOM20 and inhibits mitochondrial protein import in Parkinson's disease. *Sci Transl Med.* 2016;8:342ra378.
 28. Grassi D, Howard S, Zhou M, Diaz-Perez N, Urban NT, Guerrero-Given D, et al. Identification of a highly neurotoxic alpha-synuclein species inducing mitochondrial damage and mitophagy in Parkinson's disease. *Proc Natl Acad Sci U S A.* 2018;115:E2634–43.
 29. Erskine D, Koss D, Korolchuk VI, Outeiro TF, Attems J, McKeith I. Lipids, lysosomes and mitochondria: insights into Lewy body formation from rare monogenic disorders. *Acta Neuropathol.* 2021;141:511–26.
 30. Shahmoradian SH, Lewis AJ, Genoud C, Hench J, Moors TE, Navarro PP, et al. Lewy pathology in Parkinson's disease consists of crowded organelles and lipid membranes. *Nat Neurosci.* 2019; 22:1099–109.
 31. Hou X, Fiesel FC, Truban D, Castanedes Casey M, Lin WL, Soto AI, et al. Age- and disease-dependent increase of the mitophagy marker phospho-ubiquitin in normal aging and Lewy body disease. *Autophagy.* 2018;14:1404–18.
 32. Xue Y, Ouyang K, Huang J, Zhou Y, Ouyang H, Li H, et al. Direct conversion of fibroblasts to neurons by reprogramming PTB-regulated microRNA circuits. *Cell.* 2013;152: 82–96.
 33. Fiesel FC, Ando M, Hudec R, Hill AR, Castanedes-Casey M, Caulfield TR, et al. (Patho-)physiological relevance of PINK1-dependent ubiquitin phosphorylation. *EMBO Rep.* 2015; 16:1114–30.
 34. Moussaud S, Malany S, Mehta A, Vasile S, Smith LH, McLean PJ. Targeting alpha-synuclein oligomers by protein-fragment complementation for drug discovery in synucleinopathies. *Expert Opin Ther Targets.* 2015;19:589–603.
 35. Livak KJ, Schmittgen TD. Analysis of relative gene expression data using real-time quantitative PCR and the 2^{-ΔΔC_T} method. *Methods.* 2001;25:402–8.
 36. Sasaki A, Arawaka S, Sato H, Kato T. Sensitive western blotting for detection of endogenous Ser129-phosphorylated alpha-synuclein in intracellular and extracellular spaces. *Sci Rep.* 2015;5: 14211.
 37. Lee BR, Kamitani T. Improved immunodetection of endogenous alpha-synuclein. *PLoS One.* 2011;6:e23939.
 38. Masliah E, Rockenstein E, Veinbergs I, Mallory M, Hashimoto M, Takeda A, et al. Dopaminergic loss and inclusion body formation in alpha-synuclein mice: implications for neurodegenerative disorders. *Science.* 2000;287:1265–9.
 39. Koga S, Ikeda A, Dickson DW. Deep learning-based model for diagnosing Alzheimer's disease and tauopathies. *Neuropathol Appl Neurobiol.* 2022;48:e12759.
 40. Gwinn-Hardy K, Mehta ND, Farrer M, Maraganore D, Muentner M, Yen SH, et al. Distinctive neuropathology revealed by alpha-synuclein antibodies in hereditary parkinsonism and dementia linked to chromosome 4p. *Acta Neuropathol.* 2000;99: 663–72.
 41. Ambrosi G, Ghezzi C, Sepe S, Milanese C, Payan-Gomez C, Bombardieri CR, et al. Bioenergetic and proteolytic defects in fibroblasts from patients with sporadic Parkinson's disease. *Biochim Biophys Acta.* 2014;1842:1385–94.
 42. Devine MJ, Ryten M, Vodicka P, Thomson AJ, Burdon T, Houlden H, et al. Parkinson's disease induced pluripotent stem cells with triplication of the alpha-synuclein locus. *Nat Commun.* 2011;2:440.
 43. Xilouri M, Brekk OR, Stefanis L. Alpha-synuclein and protein degradation systems: a reciprocal relationship. *Mol Neurobiol.* 2013;47:537–51.
 44. Hou X, Watzlawik JO, Cook C, Liu CC, Kang SS, Lin WL, et al. Mitophagy alterations in Alzheimer's disease are associated with granulovacuolar degeneration and early tau pathology. *Alzheimer's Dement.* 2020;17:417–30.
 45. Fujishiro H, Imamura AY, Lin WL, Uchikado H, Mark MH, Golbe LI, et al. Diversity of pathological features other than Lewy bodies in familial Parkinson's disease due to SNCA mutations. *Am J Neurodegener Dis.* 2013;2:266–75.
 46. Konno T, Ross OA, Puschmann A, Dickson DW, Wszolek ZK. Autosomal dominant Parkinson's disease caused by SNCA duplications. *Parkinsonism Relat Disord.* 2016;22(Suppl 1):S1–6.

47. Koga S, Sekiya H, Kondru N, Ross OA, Dickson DW. Neuropathology and molecular diagnosis of synucleinopathies. *Mol Neurodegener.* 2021;16:83.
48. Sarkar S, Olsen AL, Sygnecka K, Lohr KM, Feany MB. Alpha-synuclein impairs autophagosome maturation through abnormal Actin stabilization. *PLoS Genet.* 2021;17:e1009359.
49. Nakamura K, Nemani VM, Azarbal F, Skibinski G, Levy JM, Egami K, et al. Direct membrane association drives mitochondrial fission by the Parkinson disease-associated protein alpha-synuclein. *J Biol Chem.* 2011;286:20710–26.
50. Park JH, Burgess JD, Faruqi AH, DeMeo NN, Fiesel FC, Springer W, et al. Alpha-synuclein-induced mitochondrial dysfunction is mediated via a sirtuin 3-dependent pathway. *Mol Neurodegener.* 2020;15:5.
51. Wang X, Becker K, Levine N, Zhang M, Lieberman AP, Moore DJ, et al. Pathogenic alpha-synuclein aggregates preferentially bind to mitochondria and affect cellular respiration. *Acta Neuropathol Commun.* 2019;7:41.
52. Laperle AH, Sances S, Yucer N, Dardov VJ, Garcia VJ, Ho R, et al. iPSC modeling of young-onset Parkinson's disease reveals a molecular signature of disease and novel therapeutic candidates. *Nat Med.* 2020;26:289–99.
53. Ejlerskov P, Rasmussen I, Nielsen TT, Bergstrom AL, Tohyama Y, Jensen PH, et al. Tubulin polymerization-promoting protein (TPPP/p25alpha) promotes unconventional secretion of alpha-synuclein through exophagy by impairing autophagosome-lysosome fusion. *J Biol Chem.* 2013;288:17313–35.
54. Minakaki G, Menges S, Kittel A, Emmanouilidou E, Schaeffner I, Barkovits K, et al. Autophagy inhibition promotes SNCA/alpha-synuclein release and transfer via extracellular vesicles with a hybrid autophagosome-exosome-like phenotype. *Autophagy.* 2018;14:98–119.
55. Lee HJ, Cho ED, Lee KW, Kim JH, Cho SG, Lee SJ. Autophagic failure promotes the exocytosis and intercellular transfer of alpha-synuclein. *Exp Mol Med.* 2013;45:e22.
56. Martin LJ, Pan Y, Price AC, Sterling W, Copeland NG, Jenkins NA, et al. Parkinson's disease alpha-synuclein transgenic mice develop neuronal mitochondrial degeneration and cell death. *J Neurosci.* 2006;26:41–50.
57. Shaltouki A, Hsieh CH, Kim MJ, Wang X. Alpha-synuclein delays mitophagy and targeting Miro rescues neuron loss in Parkinson's models. *Acta Neuropathol.* 2018;136:607–20.
58. Peng C, Gathagan RJ, Covell DJ, Medellin C, Stieber A, Robinson JL, et al. Cellular milieu imparts distinct pathological alpha-synuclein strains in alpha-synucleinopathies. *Nature.* 2018;557:558–63.
59. Van der Perren A, Gelders G, Fenyi A, Bousset L, Brito F, Peelaerts W, et al. The structural differences between patient-derived alpha-synuclein strains dictate characteristics of Parkinson's disease, multiple system atrophy and dementia with Lewy bodies. *Acta Neuropathol.* 2020;139:977–1000.
60. Peelaerts W, Bousset L, Van der Perren A, Moskalyuk A, Pulizzi R, Giugliano M, et al. Alpha-synuclein strains cause distinct synucleinopathies after local and systemic administration. *Nature.* 2015;522:340–4.
61. Imaizumi Y, Okada Y, Akamatsu W, Koike M, Kuzumaki N, Hayakawa H, et al. Mitochondrial dysfunction associated with increased oxidative stress and alpha-synuclein accumulation in PARK2 iPSC-derived neurons and postmortem brain tissue. *Mol Brain.* 2012;5:35.
62. Oliveras-Salva M, Macchi F, Coessens V, Deleersnijder A, Gerard M, Van der Perren A, et al. Alpha-synuclein-induced neurodegeneration is exacerbated in PINK1 knockout mice. *Neurobiol Aging.* 2014;35:2625–36.
63. Norris KL, Hao R, Chen LF, Lai CH, Kapur M, Shaughnessy PJ, et al. Convergence of parkin, PINK1, and alpha-synuclein on stress-induced mitochondrial morphological remodeling. *J Biol Chem.* 2015;290:13862–74.
64. Chung SY, Kishinevsky S, Mazzulli JR, Graziotto J, Mrejeru A, Mosharov EV, et al. Parkin and PINK1 patient iPSC-derived midbrain dopamine neurons exhibit mitochondrial dysfunction and alpha-synuclein accumulation. *Stem Cell Rep.* 2016;7:664–77.
65. Madsen DA, Schmidt SI, Blaabjerg M, Meyer M. Interaction between parkin and alpha-synuclein in PARK2-mediated Parkinson's disease. *Cell.* 2021;10:283.
66. Lim KL, Chew KC, Tan JM, Wang C, Chung KK, Zhang Y, et al. Parkin mediates nonclassical, proteasomal-independent ubiquitination of synphilin-1: implications for Lewy body formation. *J Neurosci.* 2005;25:2002–9.
67. Chung KK, Zhang Y, Lim KL, Tanaka Y, Huang H, Gao J, et al. Parkin ubiquitinates the alpha-synuclein-interacting protein, synphilin-1: implications for Lewy-body formation in Parkinson disease. *Nat Med.* 2001;7:1144–50.
68. Schlossmacher MG, Frosch MP, Gai WP, Medina M, Sharma N, Forno L, et al. Parkin localizes to the Lewy bodies of Parkinson disease and dementia with Lewy bodies. *Am J Pathol.* 2002;160:1655–67.
69. Fanning S, Selkoe D, Dettmer U. Parkinson's disease: proteinopathy or lipidopathy? *NPJ Parkinsons Dis.* 2020;6:3.
70. Sanderson JB, De S, Jiang H, Rovere M, Jin M, Zaccagnini L, et al. Analysis of alpha-synuclein species enriched from cerebral cortex of humans with sporadic dementia with Lewy bodies. *Brain Commun.* 2020;2:fcaa010.
71. Mahul-Mellier AL, Burtscher J, Maharjan N, Weerens L, Croisier M, Kuttler F, et al. The process of Lewy body formation, rather than simply alpha-synuclein fibrillization, is one of the major drivers of neurodegeneration. *Proc Natl Acad Sci U S A.* 2020;117:4971–82.
72. Killinger BA, Melki R, Brundin P, Kordower JH. Endogenous alpha-synuclein monomers, oligomers and resulting pathology: let's talk about the lipids in the room. *NPJ Parkinsons Dis.* 2019;5:23.
73. Ghanem SS, Majbour NK, Vaikath NN, Ardah MT, Erskine D, Jensen NM, et al. Alpha-synuclein phosphorylation at serine 129 occurs after initial protein deposition and inhibits seeded fibril formation and toxicity. *Proc Natl Acad Sci U S A.* 2022;119:e2109617119.
74. Mohamed NV, Sirois J, Ramamurthy J, Mathur M, Lepine P, Deneault E, et al. Midbrain organoids with an SNCA gene triplication model key features of synucleinopathy. *Brain Commun.* 2021;3:fcab223.
75. Watzlawik JO, Hou X, Fricova D, Ramnarine C, Barodia SK, Gendron TF, et al. Sensitive ELISA-based detection method for the mitophagy marker p-S65-Ub in human cells, autopsy brain, and blood samples. *Autophagy.* 2021;17:2613–28.

SUPPORTING INFORMATION

Additional supporting information can be found online in the Supporting Information section at the end of this article.

How to cite this article: Hou X, Chen TH-Y, Koga S, Bredenberg JM, Faruqi AH, Delenclos M, et al. Alpha-synuclein-associated changes in PINK1-PRKN-mediated mitophagy are disease context dependent. *Brain Pathology.* 2023;33(5):e13175. <https://doi.org/10.1111/bpa.13175>